Journal of Alloys and Compounds 509 (2011) 8042–8046

Contents lists available at ScienceDirect

Journal of Alloys and Compounds

journal homepage: www.elsevier.com/locate/jallcom

Role of Ce–Mn substitution on structural, electrical and magnetic properties of W-type strontium hexaferrites

Imran Khan [a], Imran Sadiq [a], Muhammad Naeem Ashiq [b], Mazhar-Ud-Din Rana [a,*]

[a] Department of Physics, Bahauddin Zakariya University, Multan-60800, Pakistan
[b] Department of Chemistry, Bahauddin Zakariya University, Multan-60800, Pakistan

ARTICLE INFO

Article history:
Received 15 March 2011
Received in revised form 2 May 2011
Accepted 3 May 2011
Available online 26 May 2011

Key words:
Hexaferrites
Magnetic Properties
Coercivity
Electrical Resistivity
SEM

ABSTRACT

W-type hexaferrites with nominal composition $Sr_{1-x}Ce_xCo_2Mn_yFe_{16-y}O_{27}$ ($x = 0.00, 0.02, 0.04, 0.06$ & $y = 0.0, 0.2, 0.4, 0.6$) has been synthesized by the chemical co-precipitation method. The effect of substitution of Ce at Sr & Mn at Fe site on the structural, magnetic and electrical properties has been investigated. The XRD patterns confirm single W-type hexaferrite phase and various parameters such as lattice constants (a & c), cell volume (V), crystallite size (D), X-ray density (d_x), bulk density (d_b) and porosity (P) were calculated from XRD data. The crystallite size is found in the range of 22.5–30 nm and this size is small enough to obtained suitable signal-to-noise ratio in high density recording media. The magnetic properties such as saturation magnetization, remanence, squareness ratio and coercivity were calculated from hysteresis loops and were observed to increase with increase in Ce–Mn concentration up to a certain substitution level. The resistivity showed interesting behavior with temperature, showing metal-to-semiconductor transition temperature. The increase in saturation and remanence suggest that the synthesized materials can be used in the high density recording media.

1. Introduction

Nanotechnology has achieved tremendous progress in past several decades. Recently, nanomaterials which are the materials with basic structural units, grains, particles, or other constituent components smaller than 100 nm in at least one dimension have evoked a great attention for different applications [1]. Due to their very small size and large surface area, nanomaterials are said to have interesting physical, electrical and magnetic properties that are different from that of their bulk counterparts [2,3].

Ferrites nanomaterials are considered to be very important class of magnetic materials from applications point of view. Various attempts have been made by different researchers to enhance their electrical and magnetic properties. Amongst the different ferrites nanomaterials, increasing attention has been given to W-type hexagonal ferrites with general formula $GMe_2Fe_{16}O_{27}$ (G^{2+} = Ba, Sr, La etc.; Me^{2+} = Zn, Co, Ni, Mg, Mn, etc.) due to its better magnetic properties than those of other hexagonal ferrites [4]. These hexaferrite materials with a narrow size distribution are promising enough for potential industrial applications due to their high coercivity and saturation magnetization [5]. These materials have also been found to be very useful for microwave applications due to their very low dielectric loss [6] and are preferred over other magnetic materials i.e. alloys because of their good mechanical hardness, excellent chemical stability, high electrical resistivity and reasonable cost [7–10].

The properties of these nanomaterials depend upon the composition and microstructure of the surface which are influenced by their synthesis route. Researchers attempted to substitute divalent and trivalent cations such as Cr [11], Co [12], La [13], Cu [14], Mg [15] etc. in W-type hexagonal ferrites to enhance their different properties. However in the last few years researchers divert their attention to substitute rare earth metal at various sites in the W-type hexagonal ferrites such as Y, Er, Ho, Sm, Nd, Gd, Ce [6], Dy, Nd, Pr [16], Y, Er, Ho, Sm, Nd, Gd, Ce [17], Nd [18] because these substitution changes the magnetic interactions and therefore enhances the magnetic properties [19]. Rare earth ions have typical relaxation characteristics which may affect the electromagnetic properties of ferrite magically [20].

Various techniques such as chemical co-precipitation [11], stearic acid gel [12], standard ceramic [15], citrate combustion [19] sol–gel [21] and hydrothermal method [22] have been used for the synthesis of W-type hexagonal ferrites. Amongst these different techniques chemical co-precipitation method is found to be very suitable because of its simplicity, lower cost, comparatively lower annealing temperature and annealing time to achieve the pure single phase. This technique also helps us to obtain the narrow distribution of the particles as well.

* Corresponding author. Tel.: +92 61 9210199; fax: +92 61 9210068.
E-mail address: mazharrana@bzu.edu.pk (M.-U.-D. Rana).

0925-8388/$ – see front matter © 2011 Elsevier B.V. All rights reserved.
doi:10.1016/j.jallcom.2011.05.013

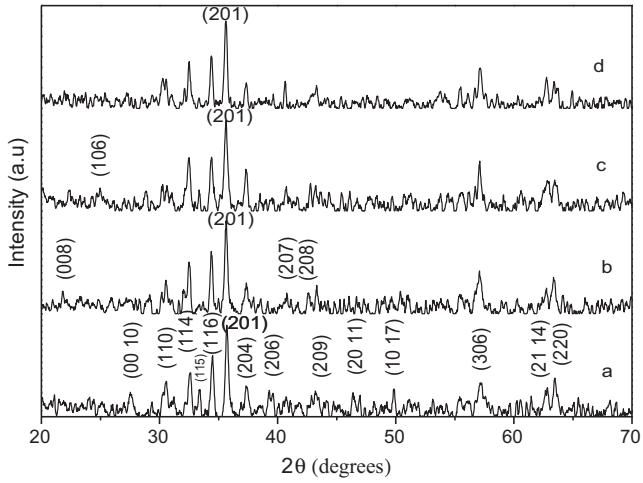

Fig. 1. X-ray diffraction patterns for $Sr_{1-x}Ce_xCo_2Mn_yFe_{16-y}O_{27}$: (a) x, $y = 0.0$, (b) $x = 0.02$, $y = 0.2$, (c) $x = 0.04$, $y = 0.4$, (d) $x = 0.06$, $y = 0.6$.

The aim of this work is to synthesize narrow size distribution of Ce–Mn doped W-type hexaferrite using simple and economic technique. The other aim is to enhance the saturation magnetization and remanence to make the material useful for high density recording media. The electrical properties of the substituted materials are also investigated in this paper.

2. Experimental

The chemicals used for the synthesis of W-type hexaferrite and its derivatives were $Fe(NO_3)_3{\cdot}9H_2O$ (Sigma Aldrich, 98%), $Sr(NO_3)_2$ (Fluka, 99%), $Co(NO_3)_2{\cdot}6H_2O$ (Philip Harris, 96%), $Ce(NO_3)_3{\cdot}6H_2O$ (Merck, 98.5%), $MnCl_2{\cdot}4H_2O$ (Peking Chemical, 98%) and NaOH (Fluka, ≥97%) and were used as such without further treatment. The stoichiometric amount of the metal salts was dissolved in deionized water and was mixed in a beaker. The solution mixture was then heated up to 60 °C with continuous stirring. When the temperature of the mixture solution reaches to 60 °C then 2M NaOH solution was added drop wise to form the precipitate. The pH of the solution was kept between 11 and 12. After the addition of NaOH continuous stirring for 3 h was maintained in order to control the crystallite size and homogeneity of the samples. The precipitates were then washed with deionized water till the pH of solution reduced to a value of 7. All the samples were then dried at 150 °C in an oven. The powdered samples were pressed into pellets of 7 mm diameter at a pressure of ~35 kN. The pellets were then annealed at a temperature of 1100 °C in box furnace (Heraeus, D-6450 Hanau, Germany) for 2 h.

The X-ray diffraction patterns were recorded using JEOL JDX-3532 diffractometer at 40 kV/30 mA. The radiation used was Cμ K_α ($\lambda = 1.5406$ Å) with Ni filter. Temperature dependent resistivity of all the samples were measured by two probe method in the temperature range of 298–673 K using source meter (Keithley-2400). SEM (Hitachi SU1510) was used to examine the morphology of all the samples. The magnetic properties such as H_c, M_s & M_r were measured at room temperature at maximum available field of 10 kOe using vibrating sample magnetometer (Lakshore-7407).

3. Results and discussions

3.1. Structure and morphology of samples

The XRD patterns of all the synthesized samples are shown in Fig. 1. All the peaks are perfectly matched with the standard pattern (ICSD 00-054-0106) confirming that there is no secondary phase. The lattice constants (a & c), cell volume (V_{cell}) and X-ray density ($d_{X\text{-ray}}$) are calculated from XRD data using following relations [11]:

$$\frac{1}{d^2_{h\,k\,l}} = \frac{4(h^2 + hk + k^2)}{3a^2} + \frac{l^2}{c^2} \quad (1)$$

$$V_{cell} = a^2 c \ \sin 120 \quad (2)$$

$$d_{X\text{-ray}} = \frac{2M}{N_A V_{cell}} \quad (3)$$

where, $d_{h\,k\,l}$ is the d-spacing and h, k and l are the corresponding miller indices, M is the molar mass of the sample and N_A is the Avogadro's number and the values of all these parameters are given in Table 1. It is clear from Table 1 that the values of lattice constants (a & c) and cell volume increase with the increase in Ce^{3+} and Mn^{2+} concentration in W-type hexaferrite while that of X-ray density decreases. The increase in both the parameters i.e. lattice constant and cell volume is due to larger ionic radius of the doped Mn^{2+} (0.80 Å) than that of host Fe^{3+} (0.64 Å). The decrease in X-ray density may be due to the increase in cell volume of the respective samples as the cell volume is inversely related to the X-ray density (Eq. (3)). The other reason for the decrease in X-ray density is due to the fact that the molecular mass of doped samples (Mn^{2+} = 55 amu) is smaller than that of the undoped sample (Fe^{3+} 56 amu).

The bulk density was calculated using following equation [11]:

$$d_{bulk} = \frac{m}{\pi r^2 h} \quad (4)$$

where, m is the mass of the pellet, r is the radius of pellet and h is the thickness of the pellet. The bulk density of the substituted samples is greater than that of the undoped (Table 1). The larger value of bulk density may be attributed to larger density of Ce^{3+} (6.78 g/cm^3) as compared to that of Sr^{2+} (2.6 g/cm^3). The bulk density is less than theoretical density (Table 1) due to the presence of pores created during sintering process [9]. The porosity of all the samples was calculated using the following relation [11]:

$$P = \frac{1 - d_b}{d_x} \quad (5)$$

where d_b is the Bulk density and d_x is the X-ray density. Table 1 shows that the porosity decreases with the substitution of Ce^{3+} & Mn^{2+} concentration which is due to increase in bulk density of the substituted materials. This shows that substitution cause densification of the strontium hexaferrite matrix [23].

The crystallite size is calculated by Debye–Scherer formula [11]:

$$D = \frac{K\lambda}{\beta \ \cos\theta_B} \quad (6)$$

where K is the shape constant having a value of 0.89 for hexagonal system, λ the wavelength of the X-rays used, β is the broadening of diffraction line measured at half width of its maximum intensity and θ_B is the Bragg's angle of diffraction. The crystallite size is found in the range of 22.5–30 nm (Table 1). It has been reported that the crystallite size <50 nm is required to obtain the suitable signal-to-noise ratio in the high density recording media [24]. In the present work the crystallite size is 22.5–30 nm so these materials can be used for applications in high density recording media in obtaining suitable signal-to-noise ratio.

Fig. 2 exhibits SEM images of all the samples of different compositions. Fig. 2(a) shows the SEM image of undoped sample indicating that the crystallites are in larger size and are agglomerated. Some rice shaped nanoparticles were observed for the sample having composition with lower substitution i.e. $x = 0.02$, $y = 0.2$ (Fig. 2(b)). The particles size become smaller and the particles are homogeneously distributed as we increase the substitution up to $x = 0.04$, $y = 0.4$ and $x = 0.06$, $y = 0.6$ as shown in Fig. 2(c and d), respectively. The shape of the materials is very important for various applications in different field and it has been reported that the rice shaped hexaferrite can be used in catalysis, information storage, surface enhanced Raman scattering, imaging and sensing [25,26].

3.2. Electrical properties

The DC electrical resistivity of the synthesized samples was measured by two probe method in the temperature range of 298–673 K. Fig. 3 shows the plot of room temperature electrical

Table 1
The values of different parameters calculated for $Sr_{1-x}Ce_xCo_2Mn_yFe_{16-y}O_{27}$ containing different Ce and Mn contents.

Parameters	$x = 0.0$, $y = 0.0$	$x = 0.02$, $y = 0.2$	$x = 0.04$, $y = 0.4$	$x = 0.06$, $y = 0.6$
Lattice constant, a (Å)	5.83	5.85	5.87	5.89
Lattice constant, c (Å)	33.30	33.52	33.84	33.94
Cell volume V (Å^3)	980	993	1010	1020
Bulk density D (g/cm^3)	2.52	2.75	2.91	2.98
X-ray density d_x (g/cm^3)	5.19	5.13	5.05	5.01
Porosity, P	0.51	0.46	0.42	0.40
Crystallite size D (nm)	30.0	22.9	22.5	30.0
Metal–semiconductor transition temp. (T_{M-S}) (K)	328	333	338	328
Squareness ratio (M_r/M_s)	0.57	0.56	0.60	0.58

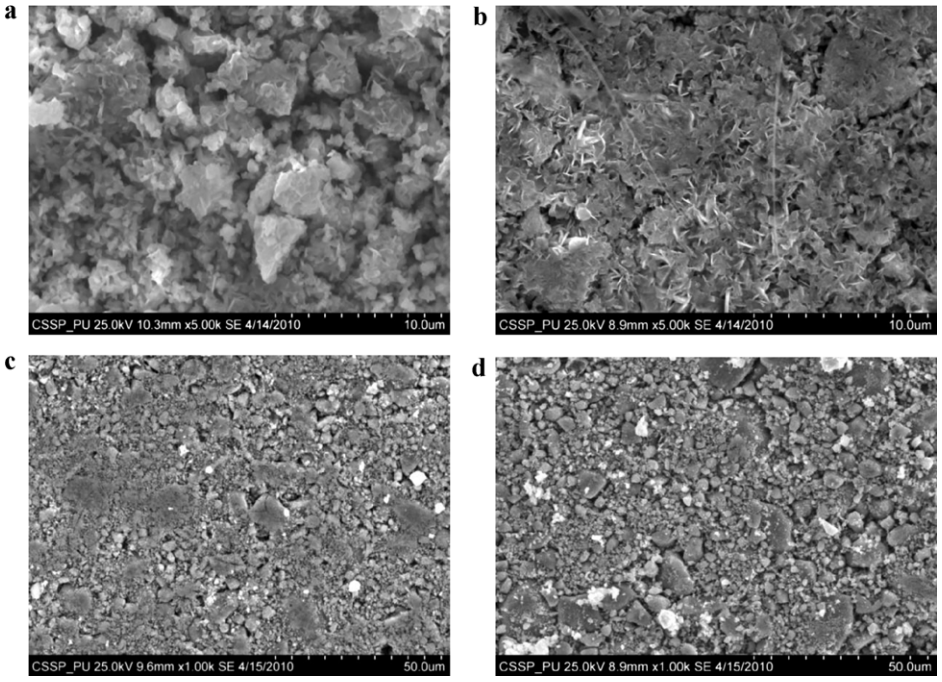

Fig. 2. SEM micrographs for $Sr_{1-x}Ce_xCo_2Mn_yFe_{16-y}O_{27}$: (a) $x, y = 0.0$, (b) $x = 0.02$, $y = 0.2$, (c) $x = 0.04$, $y = 0.4$, (d) $x = 0.06$, $y = 0.6$.

resistivity as a function of Ce–Mn content. It is observed that resistivity decreases with increasing Ce^{3+} and Mn^{2+} ions concentration. It has been reported that the conductivity in hexaferrite is due to the transfer of electrons from ferrous to ferric ions at the octahedral site [27]. It has also been reported that the substitution of Ce^{3+} at Sr^{2+} site generates the ferrous ions at the octahedral site [19]. As the number of Fe^{2+} at octahedral site is increasing with the increase in Ce^{3+} content then as a result the hopping of electrons between Fe^{3+} and Fe^{2+} ions also increase at that sites. Consequently the resistivity starts to decrease with the increase in the Ce–Mn concentration.

The variation of resistivity with temperature for all the samples is shown in Fig. 4 and shows very interesting behavior. The resistivity first increases with temperature and reaches to a maximum value at a particular temperature and then starts to decrease as expected in case of ferrites materials. The temperature at which this transition (metal to semiconductor) takes place is termed as

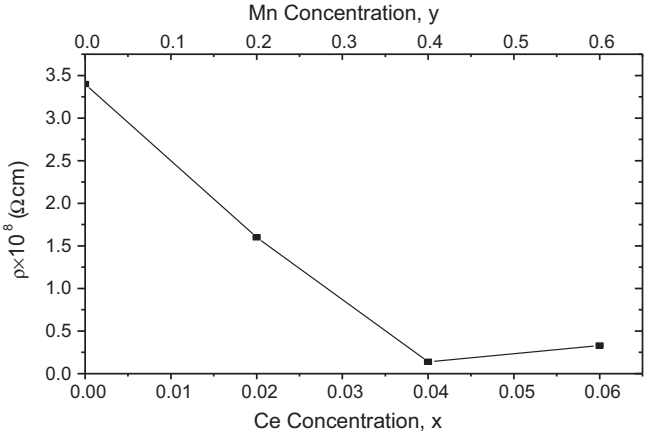

Fig. 3. Room temperature resistivity as a function of Ce^{3+}–Mn^{2+} concentration.

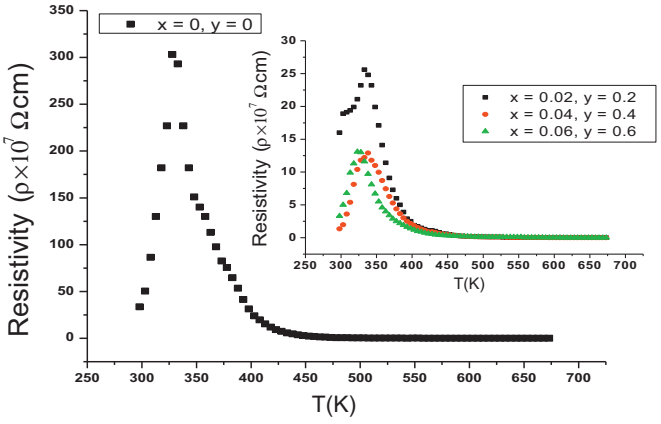

Fig. 4. Variation of electrical resistivity with temperature for $Sr_{1-x}Ce_xCo_2Mn_yFe_{16-y}O_{27}$.

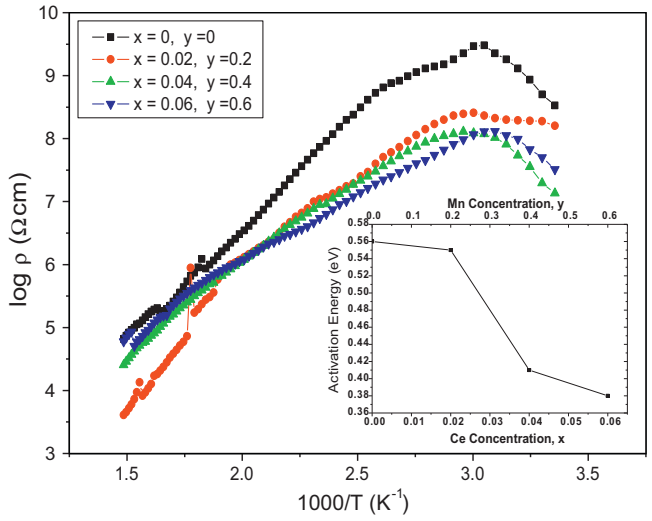

Fig. 5. (a) Plot of log ρ (Ω cm) Vs 1000/T for $Sr_{1-x}Ce_xCo_2Mn_yFe_{16-y}O_{27}$ samples for different concentrations of Ce and Mn; (b) inset, plot of activation energy with Ce^{3+} and Mn^{2+} concentrations.

metal–semiconductor transition temperature (T_{M-S}) and its values are given in Table 1. This type of behavior is very important for switching applications [28]. Such resistivity-temperature behavior has also been reported for Cr, Al–Ga, Zr–Ni substituted hexaferrite [11,23,29]. The metallic behavior below T_{M-S} is due to the presence of adsorbed moisture at the surface of the sample [30]. The activation energy has also been calculated from the temperature dependence resistivity data using Arrhenius type equation and is shown in Fig. 5. The variation of activation energy as a function of Ce–Mn content is shown in Fig. 5 as inset. The activation energy decreases with the increase in Ce–Mn content which is due to decrease in resistivity of the substituted materials. The resistivity and activation energy data are in good agreement with each other.

3.3. Magnetic properties

The magnetic properties such as coercivity (H_c), saturation magnetization (M_s), remanence (M_r) and squareness ratio (M_r/M_s) are calculated from hysteresis loops Fig. 6. The width of the loops shows that these materials have high coercivity and are hard ferrites. The behavior of saturation magnetization (M_s), remanence (M_r) and coercivity (H_c) with increasing concentrations of Ce–Mn are shown in Figs. 7 and 8, respectively. The saturation magnetization M_s and remanence (M_r) increases initially with Ce–Mn concentration and then decreases as shown in Fig. 7. It has been observed that the rare earth substitution change the Fe^{3+} to Fe^{2+} at the octa-

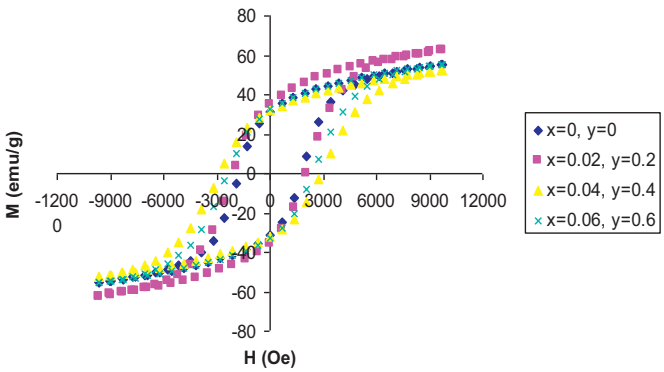

Fig. 6. Hysteresis loops for $Sr_{1-x}Ce_xCo_2Mn_yFe_{16-y}O_{27}$ samples for different concentrations of Ce and Mn.

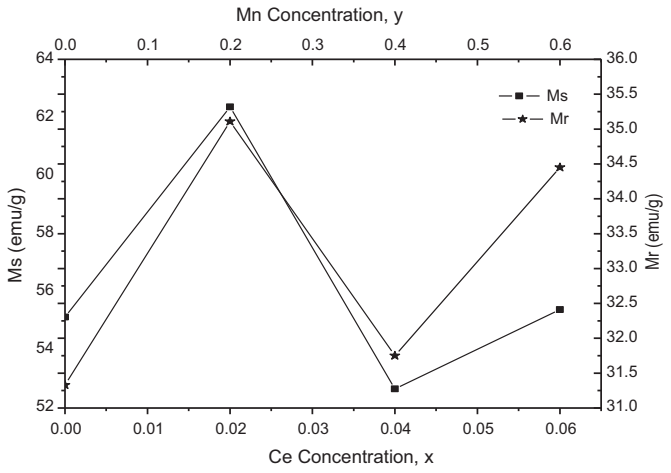

Fig. 7. Saturation magnetization and remanence as a function of Ce^{3+} and Mn^{2+} concentrations.

hedral site as discussed in resistivity part which lead to increase the Fe–O–Fe super-exchange interactions. As a result, the hyperfine field at octahedral and trigonal bi-pyramidal sites increases which is responsible for the increase in saturation magnetization and remanence. The high density recording media requires high saturation magnetization and remanence as much as possible. In the present work, the substituted sample $x = 0.02$, $y = 0.2$ has highest value of saturation magnetization and remanence. So it can be used for applications in high density recording media. The decrease in M_s and M_r at higher substitution may be due to the break up of magnetic co-linearity and spin canting. The squareness ratio (M_r/M_s) has also been calculated and its values are given in Table 1. It can be seen that the value of squareness ratio is in between 0.56 and 0.60. The value above 0.5 indicates that materials are in single magnetic domain and below 0.5 related to the multi magnetic domains. In the present work, the squareness ratio is above 0.5 suggesting that the synthesized samples are in single magnetic domain.

The value of H_c initially increases with Ce–Mn concentration till it reaches the optimum value (2856 Oe) at $x = 0.04$, $y = 0.4$ and then decreases (Fig. 8). It has been reported that the small crystallite size increase the value of coercivity [31]. In the present investigation the crystallite size decreases with the increase in Ce–Mn content (Table 1) which is responsible for the increment in the value of coercivity. The increase in coercivity is also due to change in Fe^{3+} to Fe^{2+} at octahedral site which cause to increase the magnetocrys-

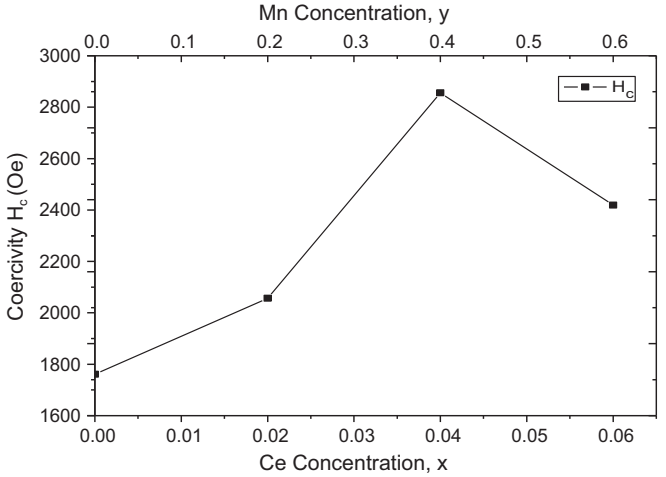

Fig. 8. Variation of Coercivity with Ce^{3+} and Mn^{2+} concentrations.

talline anisotropy. The increase in magnetocrystalline anisotropy is responsible for the increase in coercivity. The longitudinal magnetic recording media requires high enough coercivity of 600 Oe while for perpendicular magnetic recording media above 1200 Oe [32]. The coercivity value is above 1200 Oe in the present study for all the synthesized materials so these can be used in the perpendicular recording media.

4. Conclusion

Ce–Mn substituted W-type strontium ferrites were prepared by a simple chemical co-precipitation method. The XRD data clarify that all the synthesized samples have single W-type hexa phase and crystallite size is found enough small to attain the suitable signal to noise ratio. Room temperature resistivity decreases with increasing Ce^{3+} & Mn^{2+} ions concentration, which may be due to the fact that the substitution of Ce^{3+} at Sr^{2+} site increases the concentration of Fe^{2+} ions at octahedral site. Saturation magnetization and remanence increase with Ce–Mn concentration which suggests that the synthesized material can be used for applications in high density recording media. The increase in the value of coercivity >1760 Oe suggests that the synthesized samples are better to use for perpendicular magnetic recording media.

Acknowledgement

One of the authors (Imran Khan) is highly thankful to Higher Education Commission (HEC) of Pakistan for financial support for this work under Indigenous Scholarship 5000 Scheme.

References

[1] D.S. Mathew, R.S. Juang, Chem. Eng. J. 129 (2007) 51–65.
[2] H. Gleiter, Prog. Mater. Sci. 339 (1989) 223.
[3] H.J. Fendler, Chem. Rev. 87 (1987) 877.
[4] F. Leccabue, R. Painzzieri, G. Albanese, G. Leo, N. Suarez, Mater. Res. Bull. 33 (1988) 263.
[5] T.O. Kuzmitchera, L.P. Opkhovik, V.P. Shabatin, IEEE Trans. Magn. 31 (1995) 800.
[6] M.A. Ahmed, N. Okasha, R.M. Kershi, Mater. Chem. Phys. 113 (2009) 196–201.
[7] R. Peelamedu, C.A. Grimes, D. Agrawal, R. Roy, J. Mater. Res. 18 (2003) 2292.
[8] A.K.M.A. Hossain, M. Seki, T. Kawai, H. Tabata, J. Appl. Phys. 96 (2004) 1273.
[9] M.S. Niasari, F. Davar, T. Mahmoudi, Polyhedron 28 (2009) 1455.
[10] T. Hyeon, Y. Chung, J. Park, S.S. Lee, Y.W. Kim, B.H. Park, J. Phys. Chem. B 106 (2002) 6831.
[11] M.J. Iqbal, R.A. Khan, J. Alloys Compd. 478 (2009) 847–852.
[12] X.H. Wang, T.L. Ren, L.Y. Li, L.S. Zhang, J. Magn. Magn. Mater. 184 (1998) 95–100.
[13] L. Hongying, Z. Haifeng, Y. Lanying, X. Jijing, G. Shucai, M. Jian, H. Guangyan, J. Rare Earths 25 (2007) 590–595.
[14] D.M. Hemeda, O.M. Hemeda, Am. J. Appl. Sci. 5 (4) (2008) 289–295, ISSN 1546-9239.
[15] M.A. Ahmed, N. Okasha, M. Oaf, R.M. Kershi, J. Magn. Magn. Mater. 314 (2007) 128–134.
[16] W. Jing, Z. Hong, B. Shuxin, C. Ke, Z. Changrue, J. Magn. Magn. Mater. 312 (2007) 310–313.
[17] M.A. Ahmed, N. Okasha, M. Oaf, R.M. Kershi, J. Magn. Magn. Mater. 320 (2008) 1146–1150.
[18] J. Xu, H. Zou, H. Li, G. Li, S. Gan, H. Guangyan, J. Alloys Compd. 490 (2010) 552–556.
[19] S. Ounnunkad, Solid State Commun. 138 (2006) 472–475.
[20] J.J. Jiang, H.Y. He, L.W. Deng, et al., J. Rare Earth Soc. 22 (5) (2004) 627.
[21] N. Rezlescu, C. Doroftei, E. Rezlescu, P.D. Popa, J. Alloys Compd. 451 (2008) 492–496.
[22] J.F. Wang, C.B. Ponton, I.R. Harris, J. Magn. Magn. Mater. 234 (2001) 233–240.
[23] M.J. Iqbal, M.N. Ashiq, P.H. Gomez, J.M. Munoz, J. Magn. Magn. Mater. 320 (2008) 881–886.
[24] S. Che, J. Wang, Q. Chen, J. Phys.: Condens. Matter. 15 (2003) L335–L339.
[25] D. Srivastava, I. Lee, Adv. Mater. 18 (2006) 2471–2475.
[26] H. Wang, D.W. Brandle, F. Le, P. Nordlander, N.J. Halas, Nano Lett. 6 (2006) 827–832.
[27] M. El-Saadawy, J. Magn. Magn. Mater. 219 (2000) 69–72.
[28] M.N. Ashiq, M.F. Ehsan, M.J. Iqbal, I.H. Gul, J. Alloys Compd. (2001).
[29] M.J. Iqbal, M.N. Ashiq, P.H. Gomez, J.M. Munoz, Scripta Mater. 57 (2007) 1093–1096.
[30] M.J. Iqbal, S. Farooq, Mater. Res. Bull. 44 (2009) 2050–2055.
[31] B.D. Cullity, Introduction Magn. Mater. 385 (1972) (Ch. 11).
[32] Y. Li, R. Liu, Z. Zhang, C. Xiong, Mater. Chem. Phys. 64 (2000) 256–259.